Momentum-dependent lifetime broadening of electron energy loss spectra: Sum rule constraints and an asymmetric rectangle toy model

C. T. Chantler[*] and J. D. Bourke

School of Physics, University of Melbourne, Parkville, Victoria 3010, Australia

Electron energy loss spectra enable a detailed quantification of the electronic loss mechanisms in a target solid, particularly in the low-energy region dominated by plasmon excitations. Models of the electronic response in condensed-matter systems are usually derived from free-electron gas or jellium models, which commonly neglect to account for the lifetime broadening of individual plasmon and single-electron excitations in a constrained, physical manner. This can lead to potentially significant errors in electron energy loss spectra and electron inelastic mean-free-path (IMFP) calculations. We develop a toy model of plasmon and single-electron excitations that incorporates lifetime broadening for each excitation in an energy- and momentum-dependent fashion. The model is physically constrained using optical and electronic sum rules. We demonstrate the necessity of asymmetric excitation broadening, and show that causally permitted variations in the broadening function can have a significant impact on the dielectric response of the material. Our developments are applied to molybdenum, and compared with previous modeling and high-precision experimental results for the IMFP at electron energies below 120 eV.

I. INTRODUCTION

Electron energy loss spectroscopy is a powerful analytic tool that utilizes the inelastic scattering of energetic electrons in order to probe detailed structural and chemical information about a target material [1]. Related techniques, such as x-ray absorption fine-structure spectroscopy [2], Auger electron spectroscopy [3], and electron microscopy [4], also rely heavily on detailed knowledge of the inelastic scattering of electrons, in particular the electron inelastic mean free path (IMFP), in order to accurately probe material properties. Recent investigations have demonstrated the particularly critical nature of low-energy electron scattering (<100 eV) in all of these techniques [5,6]. However, established theoretical and experimental methods for obtaining inelastic electron-scattering data have typically been reliable only at much higher energies [7].

We are therefore motivated to investigate the extension of theoretical models for inelastic electron scattering in the low-energy regime. We focus on a particular area of weakness in current models—the detailed representation of bulk- (plasmon) and single-electron excitations in the electron energy loss function or, equivalently, the momentum-dependent dielectric function [8].

Existing models of these excitations in bulk solids, commonly used in the determination of electron energy loss spectra, feature well-defined dispersion relations that define the resonant energy of each particular excitation as a function of its momentum [9,10]. This allows excitations triggered by electron scattering events to be inferred from known optical excitations. The dispersion relations vary significantly between models, however, and may depend on the final-state lifetime of the corresponding optical excitation [11]. This lifetime is always considered to be fixed for a given excitation

across all momenta, despite the very likely reality of shorter lifetimes for fast-moving particles.

This work utilizes a sum rule constrained toy model of momentum-dependent plasmon broadening to investigate the potential significance of a momentum-dependent excitation lifetime on electron energy loss spectra and on the electron IMFP. The model is applied to an idealized free-electron gas system, and then to elemental molybdenum in order to compare with recent high-precision experimental IMFP investigations [12].

II. THE ASYMMETRIC RECTANGLE MODEL

A. Optical data models

The electron energy loss function (ELF) provides a quantification of the probability of an energetic electron depositing energy $\hbar\omega$ and momentum $\hbar q$ into a condensed-matter system, resulting in plasmon or single-electron excitations. The ELF is defined as the imaginary part of the negative inverse of the complex dielectric function $\epsilon(q,\omega)$, i.e.,

$$\text{ELF} = \text{Im}\left[\frac{-1}{\epsilon(q,\omega)}\right]. \tag{1}$$

This expression is the principal determinant of the electron inelastic scattering cross section σ, and of the electron IMFP λ [13]. The IMFP may be evaluated directly by integration of the ELF following [14]

$$\lambda(E)^{-1} = \frac{\hbar}{a_o \pi E} \int_0^{\frac{E-E_F}{\hbar}} \int_{q_-}^{q_+} \frac{1}{q}\text{Im}\left[\frac{-1}{\epsilon(q,\omega)}\right] dq\,d\omega, \tag{2}$$

where E is the energy of the incident electron. The terms a_0 and m are the Bohr radius and electron mass, while the Fermi energy E_F is defined relative to the bottom of the conduction band. The limits of the momentum integral are given by

$$q\pm = \sqrt{\frac{2mE}{\hbar^2}} \pm \sqrt{\frac{2m}{\hbar^2}(E - \hbar\omega)}. \tag{3}$$

---

*chantler@unimelb.edu.au

Determination of the electron IMFP requires knowledge of the ELF of the scattering material, but in practice this is difficult to evaluate directly. Most commonly, the ELF is determined in the optical limit $\epsilon(0,\omega)$ via optical transmission or reflection measurements [15], electron energy loss spectroscopy (EELS), reflection EELS (REELS) [16], or inelastic x-ray scattering (IXS) [17]. Recently, theoretical determinations have also become possible via computational techniques such as density functional theory (DFT) [18].

Given data for the optical part of the ELF, one can interpret the spectrum as a sum of components corresponding to excitations in a free-electron gas (FEG). In this way, the solid can be modeled as a collection of free-electron gases with relative contributions weighted by an amplitude term A_i [19]. The ELF can then be expressed, in the optical limit $\hbar q \to 0$, as

$$\mathrm{Im}\left[\frac{-1}{\epsilon(0,\omega)}\right]_{\mathrm{data}} = \sum_i A_i \mathrm{Im}\left[\frac{-1}{\epsilon(0,\omega;\omega_p=\omega_i)}\right]_{\mathrm{FEG}}, \quad (4)$$

where $\mathrm{Im}[\frac{-1}{\epsilon(0,\omega;\omega_p=\omega_i)}]_{\mathrm{FEG}}$ is the optical ELF for a free-electron gas with plasma frequency $\omega_p = \omega_i$. Such an ELF will consist of a single resonance peak with energy $\hbar\omega_i$ and, in the case of a lossless gas, may be given by a δ function. By assigning the amplitude parameters A_i to match the optical data, we may build a momentum-dependent ELF using an existing model for a free-electron gas:

$$\mathrm{Im}\left[\frac{-1}{\epsilon(q,\omega)}\right] = \sum_i A_i \mathrm{Im}\left[\frac{-1}{\epsilon(q,\omega;\omega_p=\omega_i)}\right]_{\mathrm{FEG}}. \quad (5)$$

The model function describing $\epsilon_{\mathrm{FEG}}(q,\omega)$ (or, equivalently, $\mathrm{Im}[\frac{-1}{\epsilon(q,\omega)}]_{\mathrm{FEG}}$) is typically one of a few popular literature models such as the Drude model [20], Lindhard model [21], or Mermin model [22]. Some of these models (notably the Drude and Mermin) explicitly consider a broadening effect arising from the finite lifetime of the resonant excitation, and will therefore define components of the ELF in terms of their amplitude A_i, optical plasma frequency ω_i, and lifetime broadening γ_i. The broadening parameters are almost always held as constants, even though the lifetime broadening of a plasmon or single-electron excitation is, in fact, likely to be variable based on its energy and momentum. Some investigations have demonstrated that an explicitly momentum-dependent broadening function $\gamma_i(q)$ may significantly improve agreement with experimental data [23]; however, such an approach is not generally used, as the correct form of the momentum dependence is not presently clear.

The inclusion of the broadening term γ_i also complicates the data-matching procedure described by Eq. (4). When $\gamma_i = 0$, δ functions may be uniquely defined with amplitudes matching the optical ELF data. With excitations of finite width, however, there potentially exist many possible ways to fit the optical spectrum, and thus the parameters A_i, ω_i, and γ_i are not uniquely defined. This may result in a large range of potential values for the ELF at high values of momentum transfer $\hbar q$.

B. Excitation broadening and sum rules

These problems may be addressed with the implementation of a causally constrained momentum-dependent lifetime $\gamma_i(q)$

assigned to each excitation. In order to evaluate the impact of such a parameter on the ELF, we may investigate a relatively simple toy model of the free-electron gas components, constrained by the Thomas-Reiche-Kuhn and Kramers-Kronig sum rules [24]. The Thomas-Reiche-Kuhn rule, also commonly known as the f-sum rule, is given by

$$\frac{\pi}{2}\omega_i^2 \approx \int_0^\infty \omega \mathrm{Im}\left[\frac{-1}{\epsilon(\omega)}\right] d\omega. \quad (6)$$

This rule is generally applicable to all values of momentum transfer $\hbar q$, and is commonly used to evaluate the consistency of measured and calculated optical dielectric data [25]. The expression we are using applies to a single oscillator, or a free-electron gas with a well-defined resonance frequency ω_i. For a general material with several resonance peaks, the plasma frequency must be replaced using $\omega_i = (4\pi ne^2/m)^{1/2}$, where n is the density of electrons in the material. In this work, we are interested solely in the momentum dependence of the ELF, and so we will assume that any optical data that we use are already compliant with the f-sum rule. This allows us to focus only on ensuring that the value of the f sum, defined by the right-hand side (RHS) of Eq. (6), is self-consistent across all momenta.

The Kramers-Kronig, or KK-sum rule, is given by

$$1 + \mathrm{Re}\left[\frac{-1}{\epsilon(q,0)}\right] = \frac{2}{\pi}\int_0^\infty \frac{1}{\omega}\mathrm{Im}\left[\frac{-1}{\epsilon(q,\omega)}\right] d\omega. \quad (7)$$

This rule is also applicable across all momenta; however, the left-hand side of the expression can be ill defined for $q \neq 0$. We therefore make an approximation following the Drude dielectric theory, which represents the real component of the inverse dielectric function in terms of ω_q, the resonant or peak energy of an excitation at momentum $\hbar q$ [26]:

$$\mathrm{Re}\left[\frac{-1}{\epsilon(q,0)}\right] \approx \frac{\omega_i^2}{\omega_q^2} - 1. \quad (8)$$

This allows us to rewrite the KK-sum rule as

$$\frac{\pi}{2}\omega_i^2 \approx \omega_q^2 \int_0^\infty \frac{1}{\omega}\mathrm{Im}\left[\frac{-1}{\epsilon(q,\omega)}\right] d\omega, \quad (9)$$

where again we find a constraint that the right-hand side of the expression must remain constant across all momenta. In general, the behavior of an excitation typically follows some kind of dispersion relation, whereby the resonant energy of the excitation is related to its momentum following some functional form g such that

$$\omega_q = g(q,\omega_i). \quad (10)$$

A simple approximation for g, sometimes used in Drude theories, is that of a free particle:

$$g(q,\omega_i) = \omega_i + \frac{\hbar q^2}{2m}. \quad (11)$$

Whatever form g may take, it is apparent that as the energy of the excitation changes with its momentum, so too must its amplitude change in order to continue to satisfy the sum rules. Further, whatever functional form one takes for the ELF of the free-electron gas component, this change in amplitude must counteract an equal change in both the f-sum and KK-sum

values. We therefore infer the following condition for any model of the dielectric function:

$$\frac{\int_0^\infty \omega \text{Im}\left[\frac{-1}{\epsilon(0,\omega)}\right]d\omega}{\int_0^\infty \omega \text{Im}\left[\frac{-1}{\epsilon(q,\omega)}\right]d\omega} = \frac{\omega_i^2 \int_0^\infty \frac{1}{\omega}\text{Im}\left[\frac{-1}{\epsilon(0,\omega)}\right]d\omega}{\omega_q^2 \int_0^\infty \frac{1}{\omega}\text{Im}\left[\frac{-1}{\epsilon(q,\omega)}\right]d\omega}. \quad (12)$$

This expression may be simplified further for any model that represents resonances in the optical limit as δ functions. Although it is generally unphysical for a resonance to correspond to a δ function due to its implied infinite lifetime, such a modeling is not necessarily unphysical as the optical limit is itself an idealization, existing in the realm of zero momentum. A model which constrains $\gamma_i = 0$ in the optical limit may still include finite lifetime resonances for finite momenta, and can also be used to uniquely parameterize the optical ELF following Eq. (4). For such a model, we may write the following powerful condition constraining the dielectric function:

$$\frac{1}{\omega_q}\int_0^\infty \omega \text{Im}\left[\frac{-1}{\epsilon(q,\omega)}\right]d\omega = \omega_q \int_0^\infty \frac{1}{\omega}\text{Im}\left[\frac{-1}{\epsilon(q,\omega)}\right]d\omega. \quad (13)$$

C. Symmetric rectangular broadening

We can use a simple example to illustrate how these sum rule restrictions can be used to develop a formalism involving a q-dependent plasmon broadening width $\gamma(q)$. The simplest arbitrary form possible for a single plasmon resonance making up an ELF would be that of a rectangular function defined as follows:

$$\text{Im}\left[\frac{-1}{\epsilon(q,\omega)}\right] = \begin{cases} \frac{A_i}{\gamma_i \omega_q} & \text{for } \omega_q - \frac{\gamma_i}{2} < \omega \leqslant \omega_q + \frac{\gamma_i}{2} \\ 0 & \text{otherwise.} \end{cases} \quad (14)$$

As before, A_i is a constant amplitude factor designed to match external data in the optical limit and γ_i is the plasmon width. ω_q is the q-dependent resonant energy for the plasmon pole given by a dispersion relation $\omega_q = g(q,\omega_i)$, where $\omega_q = \omega_i$ when $q = 0$.

In the optical limit, the ELF defined by Eq. (14) gives an f-sum rule result of A_i [RHS of Eq. (6)], and a KK-sum rule result of $\frac{A_i \omega_q}{\gamma_i} \ln \frac{\omega_q + \gamma_i/2}{\omega_q - \gamma_i/2}$ [RHS of Eq. (9)]. Note that the f-sum rule result is entirely independent of both γ_i and q. In the limit of γ_i approaching zero, the KK-sum rule result also reduces to A_i, meaning that for a lossless excitation, both the f- and KK-sum rules are consistent and independent of q.

If γ_i is finite, then the KK-sum rule will retain its ω_q, and hence q, dependence. This means that a rectangular form for plasmon resonances can never satisfy Eq. (13), and therefore can never be self-consistent for *constant and finite* broadening widths. This limitation also exists for constant and finite widths in both the Drude and Lindhard dielectric theories.

We may still attempt to satisfy the sum rule constraints with the use of a variable width $\gamma_i(q)$. This involves specifying a functional form for $\gamma_i(q)$ designed to counteract the q dependence of ω_q so that the KK-sum rule will once again yield a constant value. ω_q, however, always increases with increasing q, and thus, like increased broadening, *increases* the outcome of the KK-sum rule. Therefore, we insert a renormalization factor $N_i(q)$, where $N_i(0) = 1$ and $N_i(q > 0) < 1$,

so that the functional form for each plasmon resonance becomes

$$\text{Im}\left[\frac{-1}{\epsilon(q,\omega)}\right] = \begin{cases} \frac{N_i(q)A_i}{\gamma_i(q)\omega_q} & \text{for } \omega_q - \frac{\gamma_i}{2} < \omega \leqslant \omega_q + \frac{\gamma_i}{2} \\ 0 & \text{otherwise.} \end{cases} \quad (15)$$

Thus we can ensure that the KK-sum rule remains constant for all values of q. However, the factor $N_i(q)$ changes the value of the f-sum rule, while the broadening we have included, due to its inherent symmetry, does not. Therefore, for any model under which the plasmon width is defined as zero in the optical limit, the plasmon broadening included at finite momentum transfer *cannot be symmetric*.

D. Asymmetric rectangular broadening

An asymmetric broadening is the only way in which we can ensure that the effect of broadening, like the effect of the renormalization factor $N_i(q)$, changes the outcome of the KK-sum rule and the outcome of the f-sum rule *by the same amount*. For our example plasmon equation, this means we must rewrite Eq. (15) as

$$\text{Im}\left[\frac{-1}{\epsilon(q,\omega)}\right] = \begin{cases} \frac{N_i(q)A_i}{\gamma_i(q)\omega_q} & \text{for } \omega_q - \alpha_i(q) < \omega \leqslant \omega_q + \beta_i(q) \\ 0 & \text{otherwise,} \end{cases} \quad (16)$$

where $\alpha_i(q) + \beta_i(q) = \gamma_i(q)$, and $\alpha_i(q) \neq \beta_i(q) \; \forall q \neq 0$. The aim is then to construct $\alpha_i(q)$ and $\beta_i(q)$ so that the broadening they invoke affects the two sum rules equally, thus ensuring satisfaction of Eqs. (12) and (13) for all values of q. We define the renormalization factor as

$$N_i(q) = \frac{\int_0^\infty \omega \text{Im}\left[\frac{-1}{\epsilon(0,\omega)}\right]d\omega}{\int_0^\infty \omega \text{Im}\left[\frac{-1}{\epsilon(q,\omega)}\right]d\omega}. \quad (17)$$

Since we have defined an explicit form for our excitations [Eq. (16)], we can substitute into Eq. (13) to find an expression for the width parameters $\alpha_i(q)$ and $\beta_i(q)$:

$$1 + \frac{\beta_i(q)^2 - \alpha_i(q)^2}{2\omega_q[\alpha_i(q) + \beta_i(q)]} = \frac{\omega_q}{\alpha_i(q) + \beta_i(q)} \ln\left[\frac{\omega_q + \beta_i(q)}{\omega_q - \alpha_i(q)}\right]. \quad (18)$$

This relationship is satisfied by the trivial case of $\alpha_i(q) = \beta_i(q) = 0$, corresponding to a partial pole or lossless plasmon model [27]. We can also find an expression for $N_i(q)$ by combining Eqs. (16) and (17), yielding

$$N_i(q) = A_i \left\{\omega_q + \frac{\beta_i(q)^2 - \alpha_i(q)^2}{2[\alpha_i(q) + \beta_i(q)]}\right\}^{-1}. \quad (19)$$

We now have two equations [(18) and (19)] and three unknowns [$N_i(q), \alpha_i(q)$, and $\beta_i(q)$]. We must therefore define a third constraint, which we will construct by relating the broadening parameter $\alpha_i(q)$ to the peak resonance energy $\omega_i(q)$. In the limit of zero broadening, we must have that $\alpha_i(q) = 0, \forall q$. A second physically significant model will hold that electronic excitations will propagate only at energies higher than the plasma frequency $\omega_p = \omega_i(0)$. This second model can be defined by stating that $\alpha_i(q) = \omega_q - \omega_i$. Finally, we also wish to consider a model where excitations may exist below the

plasma frequency, implying that for $q > 0$, $\alpha_i(q) > \omega_q - \omega_i$. All of these options may be conveniently described by defining the following relationship between $\alpha_i(q)$ and $\omega_i(q)$:

$$\alpha_i(q) = \omega_q \frac{\omega_q - \omega_i}{\frac{\omega_i}{1+a_i} + \omega_q - \omega_i}. \tag{20}$$

Here we have implemented a new parameter a_i, which may be varied in order to produce each of our possible physical models. In the case of $a_i = -1$, both $\alpha_i(q)$ and $\beta_i(q)$ reduce to zero, resulting in a lossless partial pole model. For $a_i = 0$, we find that $\alpha_i(q) = \omega_q - \omega_i$. This moderate broadening model, in which excitations in the optical limit may result only in higher-energy excitations at finite momentum transfer, represents an approach similar, for example, to that of Sorini *et al.* [10]. If we increase a_i to large positive values, the resonances will broaden to encompass energies both above and below the plasma energy of the material. This behavior is qualitatively consistent with what may be expected in a Mermin model.

III. A FREE-ELECTRON GAS EXAMPLE

The most simple demonstration of how our toy model works is for the case of a free-electron gas, which consists of a single excitation that we will model as a δ function at an arbitrary energy of 30 eV in the optical limit. We show the corresponding energy and momentum ranges over which such an excitation may propagate under the asymmetric rectangle model in Fig. 1. In all cases, the energy loss function is defined by Eq. (16). The green region represents the case of a lossless plasmon, where $a_i = -1$. The blue region is determined using $a_i = 0$, corresponding to moderate losses, while the red region represents a model with $a_i = 100$, corresponding to extreme losses. In all cases, the dispersion relation $\omega_q = g(q, \omega_i)$ follows the quantum-mechanical Lindhard formulation for plasmons in a free-electron gas [21].
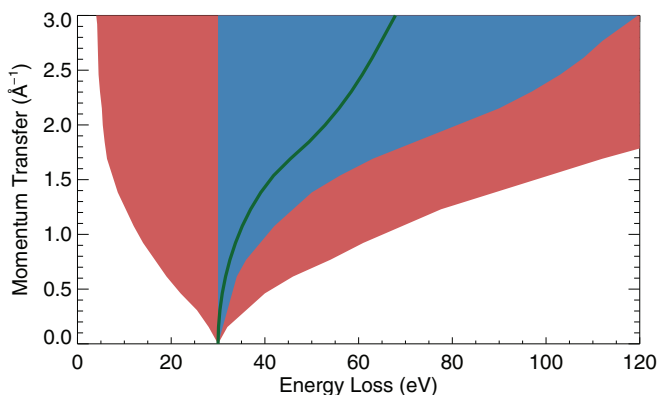
FIG. 1. (Color online) Valid energy and momentum combinations for bulk- and single-electron excitations in an ideal free-electron gas of plasma frequency $\omega_p = 30$ eV. Different colors represent results from different assumptions regarding the level of second-order losses (i.e., finite excitation lifetimes) in the material. The green line represents valid excitations in a lossless system ($a_i = -1$). The blue region represents valid excitations for a system with moderate losses ($a_i = 0$), while the regions bounded by the red areas represent valid energies and momenta for excitations in an extreme system with very short excitation lifetimes ($a_i = 100$).
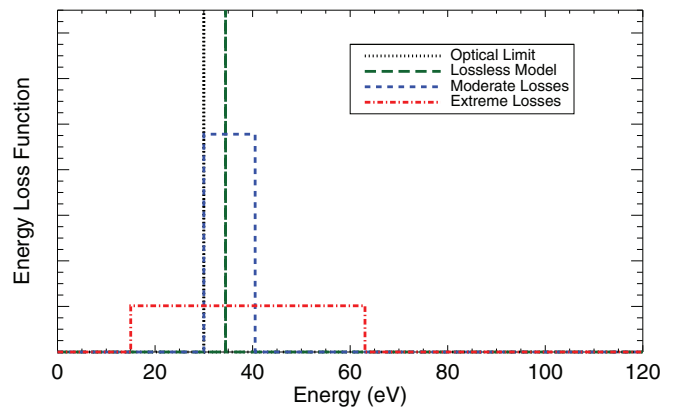
FIG. 2. (Color online) Energy loss function of an idealized system using different broadening assumptions within the asymmetric rectangle model. The dotted black line represents the loss function in the optical limit ($\hbar q = 0$), while colored curves are at $\hbar q = 1$ Å^{-1}. The green line represents an assumed lossless system ($a_i = -1$), while the blue curve assumes a system with moderate losses ($a_i = 0$), and the red curve represents a system with extreme losses ($a_i = 100$), and hence extreme excitation broadening.

Regardless of the absolute level of broadening in each case, the asymmetry of the spectrum is guaranteed by the f- and KK-sum rules. Also resulting from the sum rules is a significant reduction in the energy loss function value as the excitations are broadened. Figure 2 shows a cross section of the ELF at momentum $\hbar q = 1.0$ Å^{-1}, with the excitations modeled by asymmetric rectangles with $a_i = -1$, 0, and 100 as before. Also shown as a dotted line is the form of the excitation in the optical limit.

This momentum value (1.0 Å^{-1}) is relatively low—a determination of IMFPs over a 120 eV range, for example, requires an integration range of more than 12 Å^{-1}. The use of broadening can therefore decrease the amplitude of the ELF quite rapidly with increasing momentum transfer, and correspondingly can shift a significant amount of the potential scattering losses to both higher and lower energies. The result of this is twofold: for highly broadened systems (i.e., with low excitation lifetimes) such as when $a_i = 100$, bulk- and single-electron excitations may occur even at very low energies, leading to a dramatically lower IMFP for low-energy incident electrons. This also means that excitations will be permitted at energies below the normal cutoff determined by the plasma frequency $\hbar \omega_p$. In such systems, many losses are shifted to high energies outside of the integration range of Eq. (2), leading to an overall increase in the IMFP at high energies of the incident electron. The extent of these effects for our example free-electron gas system is shown by the IMFPs in Fig. 3.

In the extreme case of broadening quantified by $a_i = 100$, we see a dramatic reduction in the IMFP for energies below 70 eV—just over twice the energy of our assumed optical resonance. Importantly, in this case, the IMFP below 30 eV is finite, due to the existence of excitation channels for electrons with less energy than the optical resonance. This leads to a dramatic increase in the IMFP at higher energies. However, this is a most unlikely physical situation because although there is evidence in the literature to support a reduction in
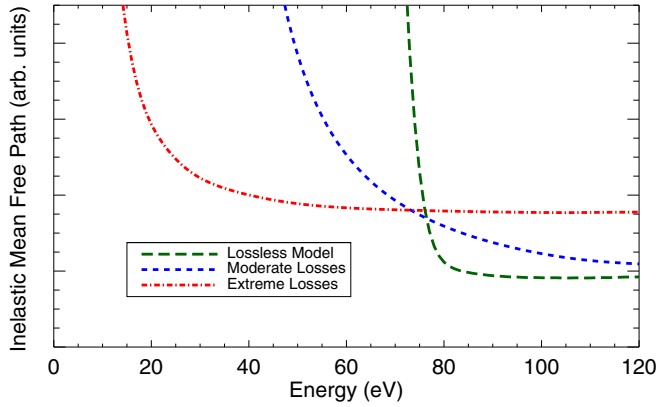
FIG. 3. (Color online) The electron IMFP of an idealized free-electron gas system of plasma frequency $\omega_p = 30$ eV. The blue line represents the IMFP for a lossless version of this system ($a_i = -1$), where bulk- and single-electron excitations have an infinite lifetime. For the red curve, the system is assumed to have moderate second-order losses ($a_i = 0$), while the green curve assumes extreme second-order losses ($a_i = 100$).

FIG. 4. (Color online) Cross sections of the ELF of molybdenum. The dotted black curve shows the optical ELF ($\hbar q = 0$), while the colored curves show the ELF at $\hbar q = 0.9$ Å^{-1}. The green curve assumes that solid Mo is lossless ($a_i = -1$), and hence retains the detailed structure of the optical ELF. The blue curve assumes moderate losses ($a_i = 0$), and the red curve assumes extreme losses ($a_i = 100$). All data are determined using the asymmetric rectangle toy model as described, with variations in the a_i parameter.

IMFP at very low energies [12,28], there is no evidence to suggest that current theories are significantly incorrect at very high energies.

The case of moderate broadening, however, is much more promising. The use of $a_i = 0$ (blue region in Fig. 1) still leads to a marked decrease in the IMFP at low electron energies, but the difference at higher energies is more subtle. This implies that a momentum-dependent broadening model may indeed be physically realistic, and also a potential tool for explaining discrepancies between theoretical and experimental data if used in an appropriate manner.

IV. APPLICATION TO MOLYBDENUM

We now turn our attention to a real-world application of the model to further assess its level of applicability. For this study, we choose molybdenum, as its electron scattering behavior has recently been studied in depth using both theoretical and high-precision experimental methods [29].

The optical ELF for Mo has also been treated in numerous studies; however, the resulting spectra have been quite varied. Recent results from density functional theory (DFT) indicate a spectrum with very strong, sharp resonance peaks around 11, 25, and 43 eV; however, data inferred from REELS measurements suggest that the 43 eV peak may in fact be much broader and less intense [16]. Another commonly used reference spectrum obtained by optical transmission measurements does not exhibit the 43 eV resonance at all [15]. Such inconsistencies are common in the tabulated optical ELF data [25], and are compounded by the sensitivity of electron-based measurements to the choice of model defining the dispersive behavior of the solid [30]. In the absence of a clear resolution to this problem, we conduct this study using theoretical data, as, first of all, it produces a better match to experiment for our final IMFP determination and, second, the existence of strongly defined peaks at higher energies allows a clearer investigation of the effect of our broadening model. We note that variations in optical data may have a significant effect

on IMFP determinations, though this is most strongly the case for variations in the ELF at very low energies corresponding to the first couple of resonances [18].

The theoretical optical ELF data is calculated using the DFT band structure package WIEN2k [31]. This package implements a linearized augmented plane-wave (LAPW) approach for solving the Kohn-Sham equation and evaluating self-consistent eigenstates for valence- and conduction-band electrons in a periodic structure. The transition amplitudes between loosely bound states are evaluated within the first Born approximation in order to determine local oscillator strengths and subsequently the dielectric function and ELF in the optical limit [25,32]. The calculation includes exchange and correlation interactions via the generalized gradient approximation (GGA) [33], but neglects quasiparticle and excitonic effects. Some parameters related to the completeness of the plane-wave set and partitioning of the cluster (e.g., effective muffin-tin radius) are adjustable in order to achieve convergence, and in some cases calculations may explicitly include local orbitals for excited states (though these have been omitted here). Some small variations in DFT calculated spectra can therefore occur, and are typically most prominent in the higher-energy part of the spectrum [18].

Figure 4 shows a cross section of our calculated ELF of molybdenum. The dotted black line represents the optical ELF determined from DFT as described, which all models are constrained to match at $\hbar q = 0$. The other curves show the ELF at $\hbar q = 0.9$ Å^{-1}, utilizing the asymmetric rectangle model with different values of a_i as before.

At this momentum transfer, the model using moderate broadening ($a_i = 0$) still retains at least some features of the optical energy loss spectrum, being three dominant resonances. For the very broad case, however, electronic losses are enabled over a wide range of energies without any significant structural dependence. As with the free-electron gas example, this serves to shift some of the potential for the material to scatter incident
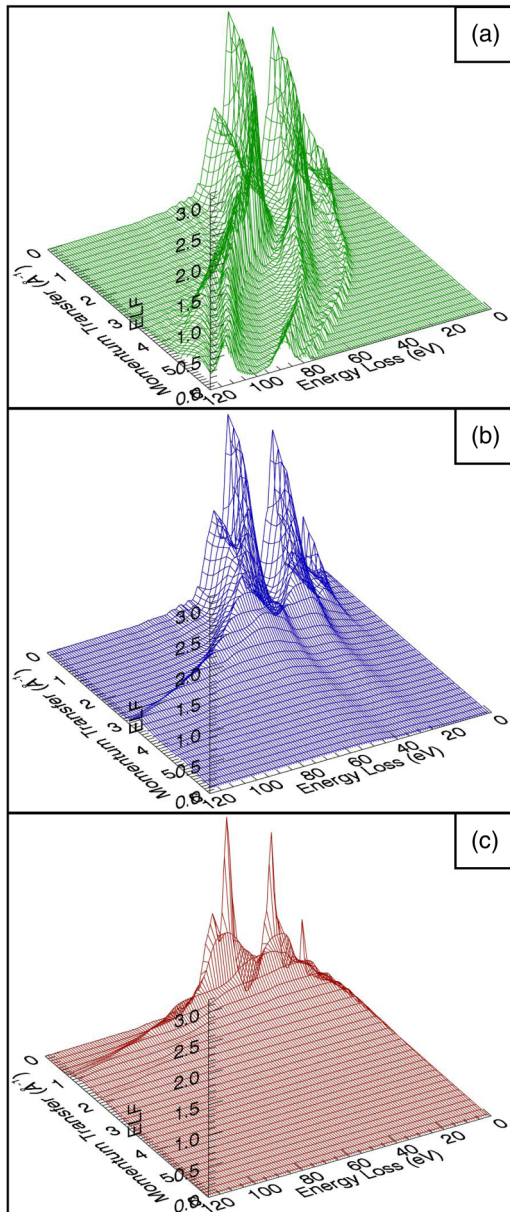
FIG. 5. (Color online) ELF of molybdenum evaluated using optical data from density functional theory, and extended via an asymmetric rectangle toy model using different assumptions regarding the overall level of excitation broadening. (a) Lossless system ($a_i = -1$); (b),(c) systems with moderate ($a_i = 0$) and extreme broadening ($a_i = 100$), respectively. The use of finite excitation broadening heavily influences both the shape and magnitude of the momentum-dependent ELF, and can enable excitations in the material below the plasma frequency ω_p.

electrons with both higher- and lower-energy transfers, causing a significant change in the electron IMFP.

We show in Fig. 5 an illustration of the energy- and momentum-dependent ELF of molybdenum over a range of momenta up to 4.0 Å^{-1}. The high rate at which the change in magnitude of the ELF occurs due to the excitation broadening is apparent. Due to the dominance of the low-energy and low-momentum region to the overall scattering, however, the effect on the IMFP is less extreme.
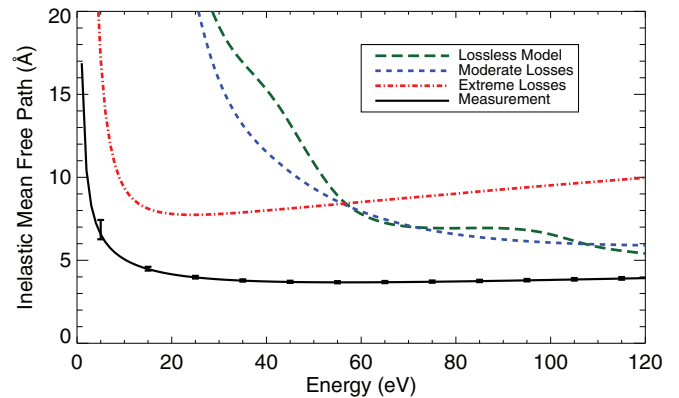
FIG. 6. (Color online) Theoretical and experimental determinations of the electron IMFP for molybdenum. The black curve with uncertainties shows a recent high-precision measurement from XAFS [12], while the colored curves show theory results from the asymmetric rectangle model. The blue curve assumes that bulk- and single-electron excitations in molybdenum are lossless ($a_i = -1$), while the red curve assumes moderate losses ($a_i = 0$), and the green curve assumes extreme losses ($a_i = 100$). The use of extreme losses appears invalid due to unphysical behavior at high energies; however, moderate losses appear physically viable, with some improvement at low energies and very small effect at high energies.

Resulting IMFP values for molybdenum are given in Fig. 6. The theoretical curves are evaluated using the ELFs plotted above from the asymmetric rectangle model using different broadening levels. These are then transformed according to Eq. (2). Also shown is the IMFP of molybdenum recently obtained by high-precision x-ray absorption fine-structure (XAFS) analysis [12].

As in the free-electron case, the use of an extreme level of broadening yields a result that is difficult to justify physically, though it does produce a marked decrease in the IMFP at low energies. The comparison between the lossless model of $a_i = -1$ and the moderate broadening model of $a_i = 0$ is much more interesting. In this regime, the broadening serves to negate the detailed oscillatory structure that otherwise appears in the theoretical result due to the highly partitioned excitation spectrum of molybdenum. Such detailed structure can appear in other modeling [12], but is usually moderated by the use of slightly broadened functions to describe the components of the ELF, rather than ideal δ functions or rectangles.

The other effects of the moderate broadening model are to change the overall magnitude of the IMFP in the high- and low-energy regions. In the high-energy region, the IMFP is only moderately increased, and over an extended energy range (i.e., keV), it may prove to be an insignificant effect, allowing continued agreement with existing theories. In the low-energy region, the IMFP is significantly reduced, reducing the discrepancy with the experimental data.

V. CONCLUSIONS

These results are strongly suggestive that the appropriate use of a causally constrained broadening algorithm to describe the behavior of bulk- and single-electron excitations may significantly reduce the current discrepancy between

theoretical and experimental electron IMFP results at low energies, without significantly affecting the established agreement at very high energies. This study has been carried out using a toy model with the simplest possible function to describe the form of excitations in the ELF (i.e., an asymmetric rectangle).

Alternate functions may produce substantially better results. These functions are limited, however, to those that can be constrained to satisfy the sum rule given by Eq. (13). These means that, for example, neither of the popular Lindhard or Drude dielectric functions can be utilized in this fashion to construct a momentum-dependent ELF in a manner that does not violate causality [34]. The Mermin function, conversely, is an asymmetric transformation of the Lindhard function that is explicitly constrained to match both the f- and KK-sum rules, and will always satisfy Eq. (13) regardless of the assigned excitation broadening. Therefore, the Mermin form is a valid trial function; however, it requires investigation as to how it may be uniquely constrained.

A very recent investigation by Da *et al.* [35] used Mermin functions with constant broadening widths in an attempt to resolve the observed discrepancy in the IMFP of molybdenum. In this case, good agreement was achieved above 80 eV by a precise match to the optical ELF using negative oscillator terms (i.e., Mermin functions with $A_i < 0$). This study demonstrates that better agreement may be obtained, but unfortunately uses negative oscillators of questionable basis to achieve this. Further, such a model compounds the problem of uniqueness in the Mermin fitting, potentially leading to a great many more free parameters.

A sequel to the current work will investigate Mermin functions, the problem of uniqueness, and constraints on energy- and momentum-dependent broadening in a fully physical model. It will demonstrate how more sophisticated modeling of the broadening function $\gamma_i(q)$ may be used to both improve the agreement with experimental results and resolve physical anomalies with the current and past theories of inelastic electron scattering.

As a final note, it is apparent from this work and others [8,18,35] that excitation broadening alone cannot fully account for the complexity of the observed discrepancy between experiment and theory at all energies. This is to be expected. Other physical factors, include the effects of exchange and correlation [36], and effective potentials from excitonic states, have been suggested recently as impacting upon the low-energy inelastic scattering behavior of electrons, despite not being routinely implemented into current theories. This work will assist in developing a body of information regarding the relative magnitude of each of these effects on the low-energy behavior of the electron IMFP. At energies above around 80 eV, it appears that the broadening effects discussed herein may yet be the dominant cause of the discrepancy [18].

ACKNOWLEDGMENTS

[1] R. F. Egerton, Rep. Prog. Phys. **72**, 016502 (2009).

[2] J. J. Rehr and R. C. Albers, Rev. Mod. Phys. **72**, 621 (2000).

[3] C. J. Powell, A. Jablonski, W. S. M. Werner, and W. Smekal, Appl. Surf. Sci. **239**, 470 (2005).

[4] B. L. Thiel and M. Toth, J. Appl. Phys. **97**, 051101 (2005).

[5] Y. Zhu, H. Inada, K. Nakamura, and J. Wall, Nat. Mater. **8**, 808 (2009).

[6] J. D. Bourke and C. T. Chantler, Phys. Rev. Lett. **104**, 206601 (2010).

[7] C. J. Powell, A. Jablonski, and F. Salvat, Surf. Interface Anal. **37**, 1068 (2005).

[8] J. D. Bourke and C. T. Chantler, J. Phys. Chem. A **116**, 3202 (2012).

[9] S. Tanuma, C. J. Powell, and D. R. Penn, Surf. Interface Anal. **43**, 689 (2011).

[10] A. P. Sorini, J. J. Kas, J. J. Rehr, M. P. Prange, and Z. H. Levine, Phys. Rev. B **74**, 165111 (2006).

[11] C. D. Denton, I. Abril, R. Garcia-Molina, J. C. Moreno-Marin, and S. Heredia-Avalos, Surf. Interface Anal. **40**, 1481 (2008).

[12] C. T. Chantler and J. D. Bourke, J. Phys. Chem. Lett. **1**, 2422 (2010).

[13] H. Nikjoo, S. Uehara, and D. Emfietzoglou, *Interaction of Radiation with Matter* (CRC Press, Boca Raton, FL, 2012).

[14] D. R. Penn, Phys. Rev. B **35**, 482 (1987).

[15] E. D. Palik, *Handbook of Optical Constants of Solids III* (Academic, New York, 1998).

[16] M. Vos, J. Elec. Spectrosc. Rel. Phenom. **191**, 65 (2013).

[17] J. Weaver, D. Lynch, and C. Olsen, Phys. Rev. B **10**, 501 (1974).

[18] C. T. Chantler and J. D. Bourke, J. Phys. Chem. A **118**, 909 (2014).

[19] C. J. Tung, J. C. Ashley, and R. H. Ritchie, Surf. Sci. **81**, 427 (1979).

[20] R. H. Ritchie and A. Howie, Philos. Mag. **36**, 463 (1977).

[21] J. Lindhard, Dan. Mat. Fys. Medd. **28**, 1 (1954).

[22] N. D. Mermin, Phys. Rev. B **1**, 2362 (1970).

[23] D. Emfietzoglou, F. A. Cucinotta, and H. Nikjoo, Radiat. Res. **164**, 202 (2005).

[24] D. Y. Smith and E. Shiles, Phys. Rev. B **17**, 4689 (1978).

[25] W. S. M. Werner, K. Glantschnig, and C. Ambrosch-Draxl, J. Phys. Chem. Ref. Data **38**, 1013 (2009).

[26] C. M. Kwei, Y. F. Chen, C. J. Tung, and J. P. Wang, Surf. Sci. **293**, 202 (1993).

[27] J. D. Bourke and C. T. Chantler, J. Elec. Spec. Rel. Phenom. **196**, 142 (2014).

[28] J. Rundgren, Phys. Rev. B **59**, 5106 (1999).

[29] C. T. Chantler and J. D. Bourke, J. Phys.: Condens. Matter **26**, 145401 (2014).

[30] M. Vos and P. L. Grande, Surf. Sci. **630**, 1 (2014).

[31] P. Blaha, K. Schwarz, G. K. H. Madsen, D. Kvasnicka, and J. Luitz, *WIEN2k, An Aug- mented Plane Wave + Local Orbitals Program for Calculating Crystal Properties* (Karlheinz Schwarz, Techn. Universität Wien, Austria, 2001).

[32] C. Ambrosch-Draxl and J. O. Sofo, Comp. Phys. Comm. **175**, 1 (2006).

[33] J. P. Perdew, K. Burke, and M. Ernzerhof, Phys. Rev. Lett. **77**, 3865 (1996).

[34] This is excepting the ideal and trivial case of a lossless system where $\gamma_i(q) = 0, \forall i, q$.

[35] B. Da, H. Shinotsuka, H. Yoshikawa, Z. J. Ding, and S. Tanuma, Phys. Rev. Lett. **113**, 063201 (2014).

[36] I. Nagy and P. M. Echenique, Phys. Rev. B **85**, 115131 (2012).